ISSN 1070-3284, Russian Journal of Coordination Chemistry, 2020, Vol. 46, No. 7, pp. 513–520. © Pleiades Publishing, Ltd., 2020.

A Keggin-Type Tungstovanadate-Based Hybrid Compound: Synthesis, Crystal Structure, and Electrocatalytic Oxidation of Ascorbic Acid

S. K. Shi[a], R. Q. Kang[a], J. L. Li[a], Y. Bai[a, *], and D. B. Dang[a, **]

[a] *Henan Key Laboratory of Polyoxometalate Chemistry, Institute of Molecular and Crystal Engineering, College of Chemistry and Chemical Engineering, Henan University, Kaifeng, 475004 P.R. China*

**e-mail: baiyan@henu.edu.cn*

***e-mail: dangdb@henu.edu.cn*

Received September 10, 2019; revised October 9, 2019; accepted November 6, 2019

Abstract—A new V-centered Keggin polyoxometalate-based inorganic-organic hybrid $(HPpz)_3[VW_{12}O_{40}]$ (**I**) (Ppz = piperazine) has been hydrothermal synthesized and characterized by IR spectroscopy, UV–Vis spectroscopy, elemental analysis and single-crystal X-ray diffraction (CIF file CCDC no. 1835683). Compound **I** belongs to the rhombohedral space group $R\bar{3}c$ and displays a three-dimensional supramolecular structure. The band gap energy value calculated for compound **I** was observed to be 1.30 eV using UV–Vis-NIR absorption spectrum. Furthermore, electrocatalytic performance of **I** has also been investigated in details.

Keywords: tungstovanadate, Keggin, crystal structure, electrocatalysis

DOI: 10.1134/S1070328420070064

INTRODUCTION

The molecular designing and crystal engineer of inorganic-organic hybrid compounds with intriguing structures and excellent performance has been attracting widespread attentions due to their potential applications, such as catalysis, adsorption, medicine and biology [1–3]. Among them, the synthesis of hybrid compounds based polyoxometalates (POMs) has become a rapidly growing multidisciplinar area. POMs not only have discrete, nanometer-sized, an unrivalled range of physical and chemical properties, but their structure and constituent elements can also be tuned finely [4–6]. Thus, POMs as an outstanding type of inorganic building blocks have already attracted a great attention. Moreover, POMs as acceptors could easily form hydrogen bond interactions to the organic donors due to thei rnumerous external oxygen atoms, which makes their use in supramolecular compounds with special structure and function quite popular [7–9].

The Keggin polyoxoanion $\{XM_{12}O_{40}\}^{n-}$ (X = heteroanion, M = W, Mo, V, Nb, Ta) with spherical motif, high symmetry and stable structureis used most extensively both in preparation and application in POM chemistry [10–12]. Although previous reports have considered that heteroanion templates play an important part in the synthesis process and performance presentation of POMs, the mechanism of it is not very clear until now [13–18]. Therefore, it is very essential to develop more POMs templated by infrequent constituent elements and explore more secrets on there lation between structures and properties.

Transition metals centered POMs structures have been studied several years for their interesting multielectron redox behavior [19–23]. Among them, vanadium centered POMs are of great research value, due tothe variable valence states of vanadium atom which are more prone to cause kaleidoscopic properties. However, only few examples of vanadium centered POMs, such as $[Me_4N]_7[VW_{12}O_{40}] \cdot 15H_2O$ and $[VW_{12-x}V_xO_{40}]^{n-}$ (x = 0, 1, 2, 3), have been reported [24–28]. In this paper, a new organic-inorganic hybrid compound $(HPpz)_3[VW_{12}O_{40}]$ (**I**) (Ppz = piperazine) has been prepared, which shows a stable 3D supramolecular structure formed by electrostatic interactions and kinds of hydrogen bonds between Keggin 12-tungs to vanadate sand protonated piperazine counterions. Electrocatalysis of compound **I** modified electrode to the electrochemical reaction of ascorbic acid (AA) was investigated by using cyclic voltammetry.

EXPERIMENTAL

Materials and method. All chemicals were of reagent grade quality obtained from commercial sources and used without further purification. Elemental analysis (C, H, and N) was carried out on a

Table 1. Crystallographic data and structure refinement for complex **I**

Parameter	Value
Formula weight	3158.58
Crystal system	Rhombohedral
Space group	$R\bar{3}c$
a, Å	13.0060(4)
α, deg	86.93
V, Å^3	2190.90(12)
Z	2
ρ_{calcd}, g cm^{-3}	4.783
$\mu(MoK_\alpha)$, mm^{-1}	31.614
T, K	296(2)
Index ranges	$-15 \le h \le 14$, $-15 \le k \le 7$, $-15 \le l \le 15$
Reflections total/unique/R_{Int}	10627/1296/0.051
Refined parameters/restraints	1296/114
R_1/wR_2[a, b] [$I > 2\sigma(I)$]	0.0383/0.0796
R_1/wR_2[a, b] (all data)	0.0344/0.0782
GOOF[c]	1.061
$\Delta\rho_{max}/\Delta\rho_{min}$, e Å^{-3}	1.63/−1.47

[a] $R_1 = \Sigma \| F_o| - |F_c\| / \Sigma |F_o|$; [b] $wR_2 = [\Sigma w(F_o^2 - F_c^2)^2 / \Sigma w(F_o^2)^2]^{1/2}$, $w = [\sigma^2(F_o^2) + (AP)^2 + BP]^{-1}$, where $P = (\mathrm{Max}(F_o^2, 0) + 2F_c^2)/3$; [c] $\mathrm{GOOF} = S = [\Sigma w(F_o^2 - F_c^2)^2/(n_{obs} - n_{param})]^{1/2}$.

Perkin-Elmer 240C analytical instrument. IR spectrum was recorded in a KBr pellet with a Nicolet 170 SXFT-IR spectrophotometer in the 4000–400 cm^{-1} region. The UV–Vis spectra in the solid state were obtained on a Shimazu UV-250 spectrometer in the range of 1500–200 nm. Electrochemical measurements were carried out on a model CHI660E electrochemical workstation (Cheng-Hua, Shanghai, China) at ambient temperature. A conventional three-electrode electrochemical system was used for all electrochemical experiments. The working electrode was a carbon paste electrode (CPE) which is made from a mixture of conducting graphite powder and a pasting liquid. A commercial Ag/AgCl electrode and a tabular Pt piece electrode were used as the reference and the auxiliary electrode, respectively.

Synthesis of $(HPpz)_3[VW_{12}O_{40}]$ (I). A mixture of NH_4VO_3 (0.048 g, 0.418 mmol), $Na_2WO_4 \cdot 2H_2O$ (0.512 g, 1.561 mmol), $Cu(CH_3COO)_2 \cdot H_2O$ (0.074 g, 0.409 mmol) and piperazine anhydrous (0.049 g, 0.250 mmol) in 10 mL deionized water was stirred at room temperature for 2 h. The pH value was adjusted to about 3.6 with 1 mol/L HCl. After stirring for 0.5 h, the resulting mixture was sealed in a 25 mL Teflon-lined stainless steel reactor and heated at 170°C for 120 h. Then the autoclave was cooled to room temperature, and dark brown rodlike-shaped crystals were isolated and washed thoroughly with distilled water. (the yield was 46%, based on W).

For $C_{12}H_{33}N_6O_{40}VW_{12}$			
Anal. calcd., %	C, 4.53	H, 0.98	N, 2.67
Found, %	C, 4.56	H, 1.05	N, 2.66

X-ray crystallographic study. A crystal of size 0.07 × 0.08 × 0.23 mm^3 was chosen for the crystallographic study and mounted on a Bruker Smart APEX II CCD diffractometer. All diffraction measurements were performed at room temperature using graphite-monochromatized MoK_α radiation (λ = 0.71073 Å). The structure was solved by direct methods and refined on F^2 by using full-matrix least-squares methods with the SHELXL-97 program [29, 30]. All non-hydrogen atoms were refined anisotropically by full-matrix least-squares techniques. All hydrogen atoms were geometrically fixed to allow riding on the parent atoms to which they are attached. The disordered O(7) and O(8) were both refined with an occupancy 0.5. Space group, lattice parameters and other relevant information are listed in Table 1, selected bond lengths and

Table 2. Selected bond lengths (Å) and bond angles (deg) of **I***

Bond	*d*, Å	Bond	*d*, Å	Bond	*d*, Å
V(1)–O(7)	1.63(2)	V(1)–O(8)	1.705(16)	W(1–O(1)	1.650(9)
W(1)–O(3)	1.901(11)	W(1)–O(4)	1.910(11)	W(1)–O(5)	1.900(10)
W(1)–O(5)$^{\#1}$	1.910(11)	W(1)–O(7)$^{\#2}$	2.417(13)	W(1)–O(8)$^{\#3}$	2.357(15)
W(2)–O(2)	1.671(9)	W(2)–O(3)	1.919(11)	W(2)–O(4)$^{\#4}$	1.905(11)
W(2)–O(6)	1.887(11)	W(2)–O(6)$^{\#3}$	1.930(11)	W(2)–O(8)	2.391(16)
W(2)–O(8)$^{\#3}$	2.398(15)				
Angle	ω, deg	Angle	ω, deg	Angle	ω, deg
O(7)V(1)O(8)	69.8(5)	O(7)V(1)O(8)$^{\#2}$	110.2(5)	O(8)$^{\#3}$V(1)O(8)	71.2(5)
O(8)$^{\#5}$V(1)O(8)	108.8(5)	O(1)W(1)O(3)	100.6(6)	O(1)W(1)O(4)	101.7(7)
O(1)W(1)O(5)	101.9(6)	O(1)W(1)O(5)$^{\#1}$	101.0(6)	O(1)W(1)O(7)$^{\#2}$	156.5(7)
O(1)W(1)O(8)$^{\#3}$	156.3(6)	O(3)W(1)O(4)	89.3(5)	O(3)W(1)O(5)$^{\#1}$	87.4(5)
O(3)W(1)O(7)$^{\#2}$	95.7(6)	O(3)W(1)O(8)$^{\#3}$	62.8(6)	O(4)W(1)O(5)$^{\#1}$	157.4(7)
O(4)W(1)O(7)$^{\#2}$	95.2(6)	O(4)W(1)O(8)$^{\#3}$	63.5(6)	O(5)W(1)O(3)	157.5(6)
O(5)W(1)O(4)	85.6(5)	O(5)$^{\#1}$W(1)O(5)	88.9(6)	O(5)W(1)O(7)$^{\#2}$	63.0(5)
O(5)$^{\#1}$W(1)O(7)$^{\#2}$	62.9(5)	O(5)W(1)O(8)$^{\#3}$	95.5(6)	O(5)W(1)O(8)$^{\#3}$	95.3(6)
O(8)$^{\#3}$W(1)O(7)$^{\#2}$	47.2(6)	O(2)W(2)O(3)	100.7(6)	O(2)W(2)O(4)$^{\#4}$	101.6(6)
O(2)W(2)O(6)	101.0(6)	O(2)W(2)O(6)$^{\#3}$	101.4(6)	O(2)W(2)O(8)	156.0(5)
O(2)W(2)O(8)$^{\#3}$	155.0(5)	O(3)W(2)O(6)$^{\#3}$	87.1(5)	O(3)W(2)O(8)$^{\#3}$	61.7(6)
O(3)W(2)O(8)	96.7(6)	O(4)$^{\#5}$W(2)O(3)	157.6(7)	O(4)W(2)O(6)$^{\#3}$	86.4(5)
O(4)$^{\#4}$W(2)O(8)	62.8(6)	O(4)W(2)O(8)$^{\#3}$	96.5(7)	O(6)W(2)O(3)	87.8(5)
O(6)W(2)O(4)$^{\#4}$	90.1(5)	O(6)W(2)O(6)$^{\#3}$	157.5(9)	O(6)W(2)O(8)$^{\#3}$	62.4(6)
O(6)W(2)O(8)	63.0(5)	O(6)$^{\#3}$W(2)O(8)	95.9(6)	O(6)W(2)O(8)$^{\#3}$	96.0(6)
O(8)W(2)O(8)$^{\#3}$	49.0(7)				

* Symmetry codes: $^{\#1}$ $x-1, y, z+1$; $^{\#2}$ $-x+2, -y+2, -z$; $^{\#3}$ $-x+1, -y+2, -z+1$; $^{\#4}$ $-x+2, -y+1, -z+1$; $^{\#5}$ $x, y-1, z+1$.

angles are given in Table 2, and geometric parameters of hydrogen bond for complex **I** are listed in Table 3.

Supplementary material for structure **I** has been deposited with the Cambridge Crystallographic Data Centre (CCDC no. 1835683; deposit@ ccdc.cam.ac.uk or www.ccdc.cam.ac.uk/conts/ retrieving.html.

RESULTS AND DISCUSSION

Hydrothermal synthesis has already been evident to be a particularly useful technique for the preparation of novel POM-based compounds. Many factors can influence the result products of a hydrothermal reaction, including initial reactants, temperature, pH value and concentrations, etc. In this paper, dark rod-like-shape crystals of **I** were isolated by the hydrothermal reaction using NH_4VO_3, $Na_2WO_4 \cdot 2H_2O$, $Cu(CH_3COO)_2$, piperazine anhydrous, and H_2O as the starting material. Moreover, comparison experiments showed that the title compound could not be obtained without addition of transition metal copper(II) material.

Single-crystal X-ray diffraction analysis reveals that the molecule structure unit of compound **I** consists of one polyoxoanion $[VW_{12}O_{40}]^{3-}$ core and three protonation of piperazine cations. As shown in Fig. 1, the structure of the polyoxoanion cluster is a well-known α-Keggin spherical structure, in which the transition metal V atom is centered in the sphere, surrounded by 12 edge-sharing and corner-sharing

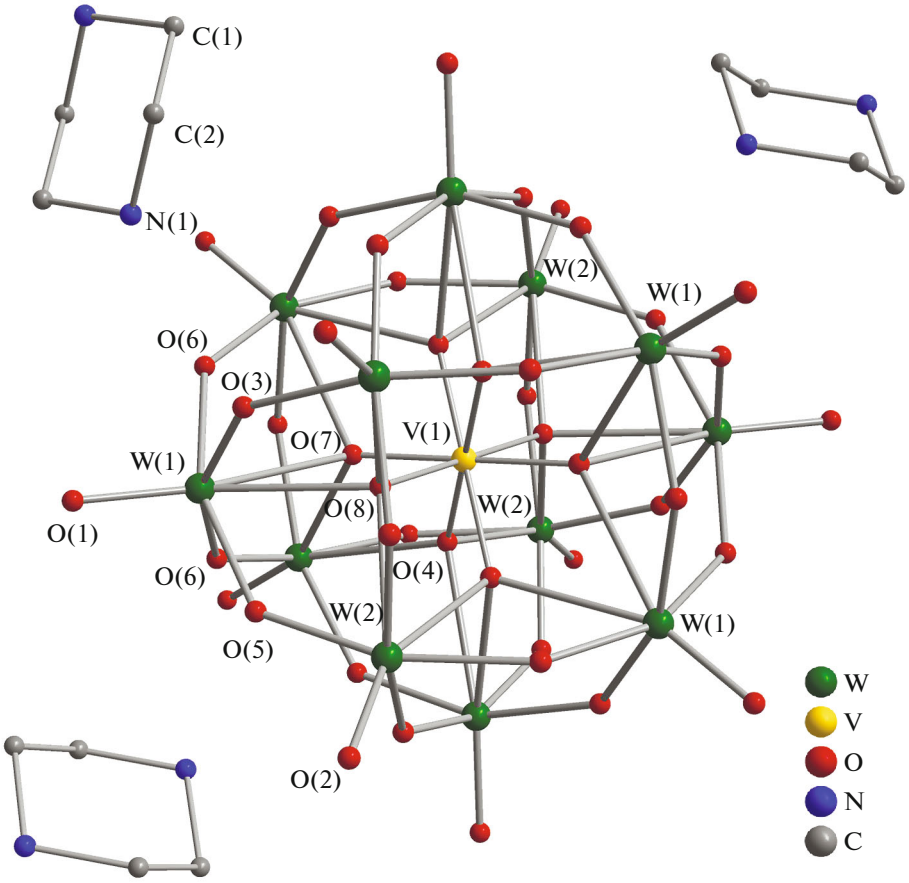

Fig. 1. Ball-and-stick representation of **I** (hydrogen atoms are omitted).

{WO_6} octahedral units. The central heteroatom V(1) and μ_4-O(8) are located on a crystallographic C_3 axis, and the site of V(1) is an inversion center in the meanwhile. Thus the four O atoms around V(1) were modelled as disordered over two orientations and exhibit a geometric symmetry with O atoms occupying eight vertices of a cube. The V–μ_4-O distances are 1.63(2) and 1.705(16) Å for O(7) and O(8), respectively (Table 2). The valence sum calculation gives that the value for vanadium is 5.50 showing the +5 oxidation state. The V–μ_4-O average distance of 1.67 Å in $[VW_{12}^{VI}O_{40}]^{3-}$ is slightly longer than that of 1.65 Å in the $[VW_9^{VI}W_3^{V}O_{40}]^{6-}$. The smaller charge on O_c (central oxygen) would affect the distance between V–O and W–O which is far off the central atom and rela-

Table 3. Geometric parameters of hydrogen bond for complex **I***

D–H···A	Distance, Å			Angle DHA, deg
	D–H	H···A	D···A	
N(1)–H(1*A*)···O(3)$^{\#6}$	0.86	2.03	2.871(17)	166
N(1)–H(1*A*)···O(5)$^{\#7}$	0.86	2.32	2.847(16)	120
C(2)–H(2*A*)···O(6)$^{\#6}$	0.97	2.55	3.218(18)	126
C(2)–H(2*A*)···O(1)$^{\#8}$	0.97	2.47	3.114(16)	124
C(2)–H(2*B*)···O(1)$^{\#9}$	0.97	2.42	3.310(16)	152

* Symmetry operations: $^{\#6}$ $3/2 - x, 3/2 - y, 1/2 - z$; $^{\#7}$ $3/2 - x, 3/2 - y, 1/2 - z$, $^{\#8}$ $1 - x, 1 - y, 1 - z$; $^{\#9}$ $-1/2 + x, 1/2 + y, 1/2 + z$.

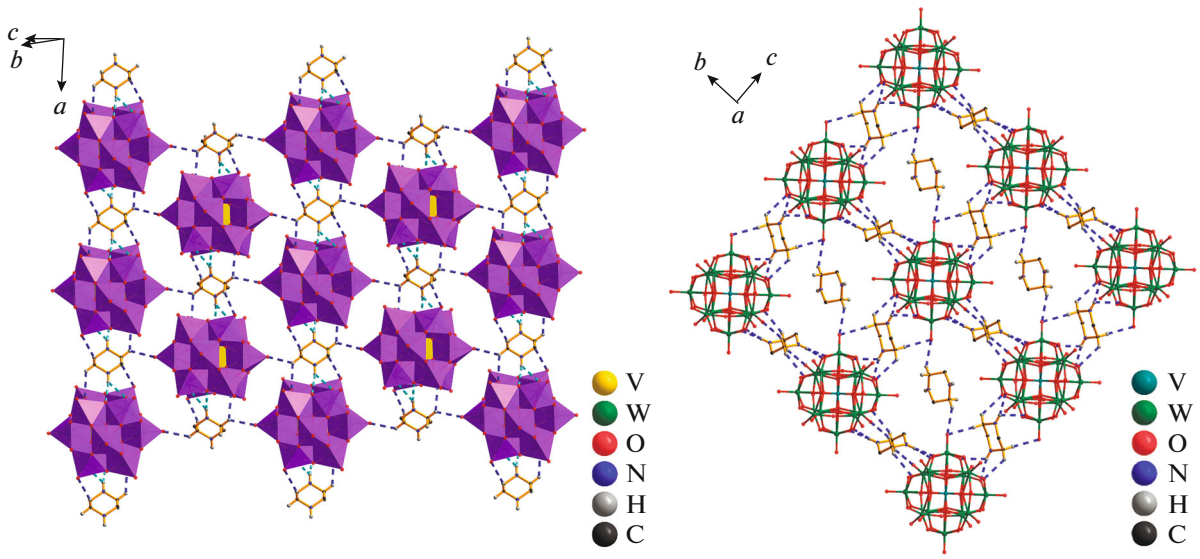

Fig. 2. The 2D architectures in compound **I**.

tively close to the nearest WO_6 octahedra [31]. The OVO angles are 108.8(5)° and 110.2(5)°. Each oxygen of the $\{VO_4\}$ group, covalently bonded to three different tungsten centers of the shell, $W-\mu_4-O_c$ distances range from 2.357 to 2.417 Å. The other two $W-O_t$ and $W-O_b$ distances are in the range of 1.65–1.671 and 1.887–1.930 Å, respectively. These values are similar to other $\{VW_{12}\}$ Keggin-type polyanions [32, 33].

Polyoxoanions having the numerous external oxygen atoms have been regarded as one type of hydrogen bond acceptors in supramolecular assembly field [34–37]. As desired, there are multiform hydrogen bonds between $[VW_{12}O_{40}]^{3-}$ polyoxoanions and protonated piperazine units (Table 2). Each protonated piperazine as hydrogen bond donor forms five types of hydrogen bonds with its neighboring oxygen atoms from two $[VW_{12}O_{40}]^{3-}$ anions. The N(1) atom and two bridging oxygen atoms O(3) and O(5) from one $[VW_{12}O_{40}]^{3-}$ anion form two N–H···O hydrogen bonds, respectively. C(2) atom forms three C–H···O hydrogen bonds with one bridging oxygen atom O(6) and two terminal oxygen atoms O(1) from three $[VW_{12}O_{40}]^{3-}$ anions. Such hydrogen bonds link the adjacent components to form a two-dimensional network (Fig. 2). Furthermore, each O(1) atom links adjacent two protonated piperazine units to extend the dimension of structure. In other words, polyanion may be as a 'template' agent to achieve the assembly of organic moieties through multiform hydrogen bonds in crystal packing, obtaining the three-dimensional supramolecular structure.

The IR spectrum of compound **I** shows several characteristic vibration patterns of α-Keggin type $[VW_{12}O_{40}]^{3-}$ polyoxoanion structure, which are similar to other 12-tungstovanadate Keggin structure [26, 27]. The medium band at 1061 cm^{-1} shows the characteristic of stretching frequency of V–O. The strong bands at 965, 879, and 776 cm^{-1} can be assigned to $\nu(W-O_t)$ (terminal oxygen), $\nu(W-O_b-W)$ (bridging oxygen), and $\nu(W-O_c-W)$ (central oxygen) [38]. In addition, the bands in 1640–1080 cm^{-1} should be attributable to Ppz ligands. The broad peak observed about 3469 cm^{-1} may correspond to the combined effect of ν(OH) and ν(NH) stretching frequency. These results were finally confirmed by X-ray crystallography.

To ensure the phase purity of the samples for further determinations, powder X-ray diffraction (PXRD) measurement of compound **I** was recorded in the range of 5°–50°. The peak positions of simulated and experimental PXRD patterns are in good agreement with each other, which suggests the good phase purity of the products.

Recently, the study of POM-base hybrids with interesting structure and excellent properties has become one of the biggest fields of POM chemistry. It is noted especially that the properties of POM-base hybrids could be adjusted by controlling organic components, thus getting promising functional materials, such as semiconductor materials, optical materials and catalysis [39–41]. Herein, to explore the conductivity potential of compound **I**, the UV–Vis-NIR absorption spectrum has been measured in the solid state. As shown in Fig. 3a, there is a particularly wide absorption band in a range of 200–1500 nm with the maximum absorption peak at about 564 nm, which can be assigned to ligand-metal charge transfer. A shoulder

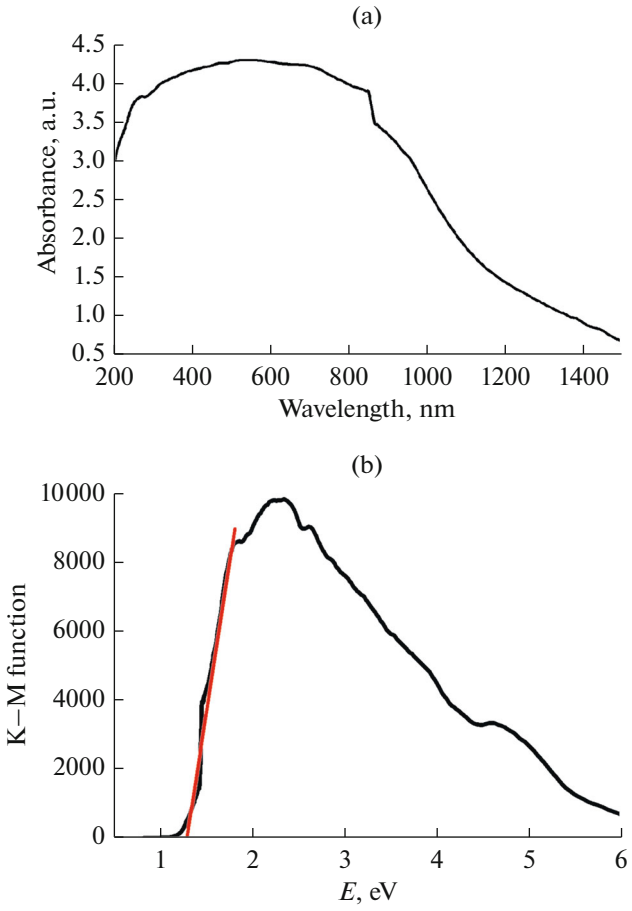

Fig. 3. The UV spectrum (a) and band gap energy (b) of compound **I** in the solid state at room temperature.

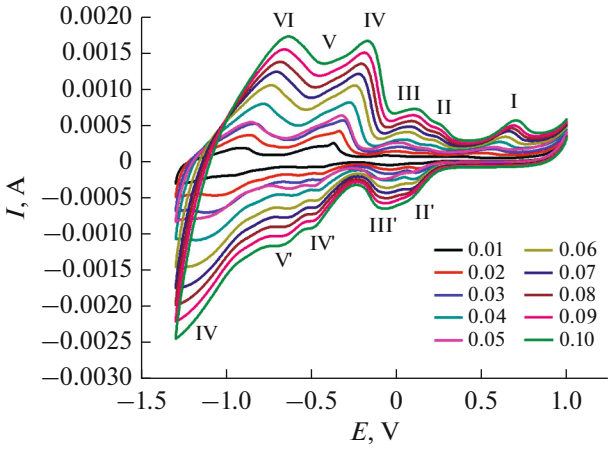

Fig. 4. The cyclic voltammograms for **I**-CPE in H_2SO_4 (0.5 M)–Na_2SO_4 (1 M) aqueous solution at different scan rates (from inner to outer: 0.01, 0.02, 0.03, 0.04, 0.05, 0.06, 0.07, 0.08, 0.09, 0.1 V s^{-1}).

peak at 263 nm can be attributed to the pπ–dπ charge transfer absorption band of $O_{b,c} \rightarrow W$. Compared with the absorption edge of about 500 nm of $[Me_4N]_7[VW_{12}O_{40}] \cdot 15H_2O$ [25], obvious red-shifted is observed for compound **I**. It is suggest that organic component may be lead to a significant contribution to optical absorption characteristic of products.

The band gap energy is a major factor determining the electrical conductivity of a solid material, which can be gained from UV–Vis-NIR absorption. The F versus E plots for compound **I** is shown in Fig. 3b, where F, Kubelka-Munk function, is $(1 - R)^2/2R$ (R, the reflectance of an infinitely thick layer at a given wavelength) [21, 42]. From this the band gap value can be assessed at 1.30 eV at room temperature, which implies the optical features of a semiconductor of compound **I**.

The electrochemical behaviors of **I**-modified carbon paste electrode (**I**-CPE) were investigated in H_2SO_4 (0.5 mol/L)–Na_2SO_4 (1 mol/L) aqueous solution at different scan rates through cyclic voltammetry (CV) method. As shown in Fig. 4, in the potential range of +1 to −1.3 V five pairs reversible redox peaks and one irreversible oxidation peak are observed for **I**-CPE at the scan rate 20 mV s^{-1}. The redox peak pairs with half-wave potentials $E_{1/2} = (E_{pa} + E_{pc})/2$ of −0.032 V (III–III'), −0.390 V (IV–IV'), −0.510 V (V–V') and −0.952 V (VI–VI') are all ascribed to the redox processes of the W^{VI} from $\{VW_{12}\}$ polyanion [43, 44]. The peak pair with $E_{1/2}$ 0.153 V (II–II') and the irreversible oxidation peak appeared in 0.501 V are attributed to the redox processes of the V center [45, 46]. With the increasing of scan rates, the anodic peak potentials and those of the corresponding cathodic peaks shift gradually in the opposite direction, indicating that redox behaviors are controlled by the surface processes [47].

In recent years, POMs acting as electrocatalyst have attracted keen interest for their multi-electron delivery and oxidation-reduction properties [48–52]. Biologic molecule dopamine (DA) and ascorbic acid (AA) have been typically applied as testing samples of electro-catalytic reactions in electro-catalytic field. Thus, electro-catalytic properties for AA have been researched by CV measurement in the 0.5 M H_2SO_4 + 1 M Na_2SO_4 aqueous solution. As is shown in Fig. 5, with addition of AA (0–25 mmol L^{-1}), the oxidation peak currents (OPCs) of **I**, **II** and **III** substantially increases and the reductive peak currents (RPCs) of **II'**, **III'** slightly decrease, suggesting the good electrocatalytic activity of **I** for the oxidation of AA [52].

FUNDING

This work was supported by the National Natural Science Foundation of China (no. 21571049), the Natural Science Foundation of Henan Province of China (nos. 162300410027, 162300410013), the Foundation of the Education Department of Henan Province of China

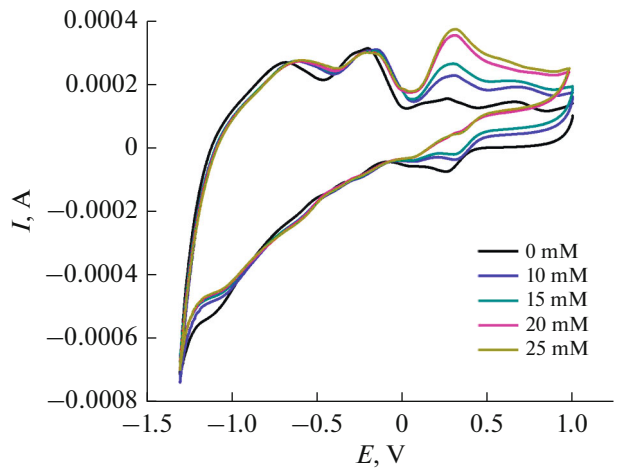

Fig. 5. Electrocatalysis of the oxidation of AA in the presence CPE-1 scan rate of 0.05 V s^{-1}. The concentrations of AA are from 0 to 25 mmol L^{-1}.

(no. 14A150022) and Open Research Funds of Henan Key Laboratory of Polyoxometalate Chemistry (HNPOMKF1607, HNPOMKF1701).

REFERENCES

1. Chen, L., Chen, W.-L., Wang, X.-L., et al., *Chem. Soc. Rev.*, 2019, vol. 48, no. 1, p. 260.
2. Misra, A., Castillo, I.F., Müller, D.P., et al., *Angew. Chem. Int. Ed.*, 2018, vol. 57, no. 45, p. 14926.
3. Folkman, S.J., Soriano-Lopez, J., Galán-Mascarós, J.R., and Finke, R.G., *J. Am. Chem. Soc.*, 2018, vol. 140, no. 38, p. 12040.
4. Chen, K. and Wu, C.-D., *Coord. Chem. Rev.*, 2019, vol. 378, p. 445.
5. Ma, X., Zhang, C., Hua, J., et al., *CrystEngComm*, 2019, vol. 21, no. 3, p. 394.
6. Korenev, V.S., Abramov., P.A., and Sokolov, M.N., *Russ. J. Inorg. Chem.*, 2018, vol. 63 p, p. 604. https://doi.org/10.1134/S003602361805008X
7. Dianat, S., Hatefi-Mehrjardi, A., and Mahmoodzadeh, K., *New J. Chem.*, 2019, vol. 43, no. 3, p. 1388.
8. Zhang, J., Huang, Y., Li, G., et al., *Coord. Chem. Rev.*, 2019, vol. 378, p. 395.
9. Ma, P., Hu, F., Wang, J., et al., *Coord. Chem. Rev.*, 2019, vol. 378, p. 281.
10. Haiduk, Yu.S., Savitsky, A.A., and Khort, A.A., *Russ. J. Inorg. Chem.*, 2019, vol. 64, p. 717. https://doi.org/10.1134/S003602361906007X
11. Korenev, V.S., Abramov, P.A., Gushchin, A.L., et al., *Russ. J. Inorg. Chem.*, 2019, vol. 64, p. 1105. https://doi.org/10.1134/S0036023619090146
12. Yang, H.-X., Zhu, W.-J., Jin, L.-Y., et al., *Russ. J. Coord. Chem.*, 2018, vol. 44, p. 466. https://doi.org/10.1134/S1070328418070035
13. Wang, X., Zhang, M.-M., Hao, X.-L., et al., *Cryst. Growth Des.*, 2013, vol. 13, no. 8, p. 3454.
14. Tong, L., Wang, Z., Xia, C., et al., *J. Phys. Chem. B.*, 2017, vol. 121, no. 46, p. 10566.
15. Chen, B. and Neumann, R., *Phys. Chem. Chem. Phys.*, 2016, vol. 18, no. 32, p. 22487.
16. Liang, Z., Sun, J., Zhang, D., et al., *Inorg. Chem.*, 2017, vol. 56, no. 17, p. 10119.
17. Huang-Fu, Y.-J., Chen, X.-Y., Yang, W., et al., *Mater. Lett.*, 2015, vol. 155, p. 48.
18. Dang, D., Bai, Y., He, C., et al., *Inorg. Chem.*, 2010, vol. 49, no. 4, p. 1280.
19. Zhao, W.-F., Zou, C., Shi, L.-X., et al., *Dalton Trans.*, 2012, vol. 41, no. 33, p. 10091.
20. Han, Z., Wang, Y., Wu, J., et al., *Solid State Sci.*, 2011, vol. 13, no. 8, p. 1560.
21. Jiao, Y.-Q., Qin, C., Zang, H.-Y., et al., *CrystEngComm*, 2015, vol. 17, no. 10, p. 2176.
22. Nakajima, K., Eda, K., and Himeno, S., *Inorg. Chem.*, 2010, vol. 49, no. 11, p. 5212.
23. Anyushin, A.V., Abramov, P.A., Gushchin, A.L., et al., *Russ. J. Inorg. Chem.*, 2017, vol. 62, no. 4, p. 397. https://doi.org/10.1134/S0036023617040027
24. Wang, J.-P., Bi, D.-Q., and Niu, J.Y., *Russ. J. Inorg. Chem.*, 2009, vol. 54, p. 403. https://doi.org/10.1134/S0036023609030127
25. Han, Z., Zhang, Q., Gao, Y., et al., *Dalton Trans.*, 2012, vol. 41, no. 4, p. 1332.
26. Khan, M.I., Cevik, S., Hayashi, R., et al., *Dalton Trans.*, 1999, vol. 10, p. 1651.
27. Han, Z.-G., Li, S., Wu, J.-J., et al., *J. Coord. Chem.*, 2011, vol. 64, no. 9, p. 1525.
28. Liu, Y., Zheng, R., Han, Z., et al., *J. Solid State Chem.*, 2015, vol. 231, p. 169.
29. Sheldrick, G.M., *SHELXL (version 5.1)*, Madison: Bruker AXS Inc., 1997.
30. Brown, I.D. and Altermatt, D., *Acta. Crystallogr., Sect. B: Struct. Sci.*, 1985, vol. 41, no. 4, p. 244.
31. Nieves, C.-P., Geoffrey, B.J., Jameson, G.B., and Baker, L.C.W., *J. Am. Chem. Soc.*, 1991, vol. 113, no. 15, p. 5658.
32. Lu, Y.-K., Cui, X.-B., Chen, Y., et al., *J. Solid State Chem.*, 2009, vol. 182, no. 8, p. 2111.
33. Lan, Q., Zhang, J., Zhang, Z.-M., et al., *Dalton Trans.*, 2013, vol. 42, no. 47, p. 16602.
34. Gong, C., Zeng, X., Zhu, C., et al., *Rsc Advances*, 2016, vol. 6, no. 108, p. 106248.
35. Xiong, J., Kubo, K., Noro, S.I., et al., *Cryst. Growth Des.*, 2016, vol. 16, no. 2, p. 800.
36. Xia, C., Wang, Z., Sun, D., et al., *Langmuir*, 2017, vol. 3, no. 46, p. 13242.
37. Tan, C. and Bu, W., *J. Solid State Chem.*, 2014, vol. 219, p. 93.
38. Yang, M.X., Lin, S., Chen, L.J., et al., *Inorg. Chem. Commun.*, 2009, vol. 12, no. 6, p. 566.
39. Li, Y.-W., Guo, L.-Y., Su, H.-F., et al., *Inorg. Chem.*, 2017, vol. 56, no. 5, p. 2481.
40. Rafiee, E., Eavani, S., et al., *Curr. Org. Chem.*, 2017, vol. 21, no. 9, p. 752.
41. Imani, A.H., Ojani, R., and Raoof, J.-B., *Int. J. Hydrogen Energy*, 2018, vol. 43, no. 17, p. 8267.

42. Li, L., Cheng, M., Bai, Y., et al., *Spectrochim. Acta, A*, 2015, vol. 150, p. 846.
43. Jamshidi, A. and Zonoz, F.M., *J. Mol. Liq.*, 2017, vol. 242, p. 993.
44. Bai, J., Li, F., Sun, Z., et al., *Inorg. Chim. Acta*, 2017, vol. 458, p. 1.
45. Wang, G., Ma, P., Zhang, D., et al., *J. Alloys Compd.*, 2016, vol. 686, p. 1032.
46. Hu, X., Xiao, Z., Huang, B., et al., *Dalton Trans.*, 2017, vol. 46, no. 26, p. 8505.
47. Zhou, W., Peng, J., Zhang, Z., et al., *Electrochim. Acta*, 2015, vol. 180, p. 887.
48. Wang, Y.F., Qin, Z.J., Tian, Z.F., et al., *J. Alloy. Compd.*, 2019, vol. 784, p. 961.
49. Qin, Z.J., Wang, Y.F., Tian, Z.-F., et al., *Mater. Lett.*, 2019, vol. 234, p. 368.
50. Han, Z.G., Zhao, Y.L., Peng, J., et al., *Electrochim. Acta*, 2005, vol. 51, no. 2, p. 218.
51. Zhang, Y., Fu, X., Zhang, C., et al., *J. Mol. Struct.*, 2018, vol. 1154, p. 543.
52. Wang, X., Zhang, S., Wang, X., et al., *Dalton Trans.*, 2017, vol. 46, no. 47, p. 16580.